OVERVIEW OF RECENT EXPERIMENTAL RESULTS ON EAST IN SUPPORT OF ITER NEW RESEARCH PLAN

X. GONG, J. HUANG, B. ZHANG, X. ZHANG, H. XU, M. WANG, J. QIAN, R. DING, M. LI, W. LIU, L. XU, P. LI, M. JIA, G. ZUO, F. DING, B. XIAO, Y. SUN, Q. ZANG, G. LI, L. WANG, H. LIU, Q. YANG, G. XU, J. HU, K. LU, Y. SONG, B. WAN, J. LI and EAST TEAM

Institute of Plasma Physics, CAS

Hefei, China

Email: xz_gong@ipp.ac.cn

A. LOARTE, R.A. PITTS, T. WAUTERS ITER Organization Sain Paul-Les-Durance, France

L. ZENG Tsinghua University Beijing, China

A. EKEDAHL IRFM/CEA Saint Paul-Les-Durance, France

Abstract

Experimental Advanced Superconducting Tokamak (EAST) has made an important advance by achieving a record H-mode plasma over 1066 seconds with the total injected energy up to 3.05GJ. A poloidal beta of $\beta_P = 2.0$ was achieved with a total RF power of 3 MW, including $P_{LHCD} = 1.1$ MW and $P_{ECRH} = 1.9$ MW and a fully non-inductive current drive with electron density at 60% of the Greenwald density, confinement enhancement factor H_{98y2} is greater than 1.3 due to the electron temperature internal transport barrier (e-ITB). Significant advancements have been made in the development of long-pulse H-mode on EAST in physics and technologies. The synergy effects between on-axis ECRH and LHCD play a crucial role in maintaining high confinement in electron channel. The long pulse H-mode discharge with e-ITB is nonlinear self-organization, emerging near the magnetic axis in a positive magnetic shear without momentum injection. In support of the R&D requirement for the ITER new research plan, a dedicated set of joint ITER-EAST experiments have been performed on optimization and characterization of boronization, plasma start-up on the tangsten limiter, and the impact of W on the H-mode operational space with and without boron-coatings. Effective Type-I ELM suppression has been achieved using n=2 RMP, these results verify a good compatibility of radiative divertor operation by injecting nitrogen. In the ~10keV high- T_i peak regime, multi-scale instabilities have been observed to provide a clear picture of the interaction between turbulence behaviors and impurity transport in the plasma core.

1. INTRODUCTION

Demonstration of high-performance long-pulse H-mode plasmas with a fusion reactor-like metal wall, low momentum input, and electron dominated heating scheme is a critical step for the success of economical fusion energy. As a superconducting tokamak, the EAST facility is uniquely positioned to contribute to resolving issues for steady state long pulse operation [1], especially with respect to radio-frequency (RF) heating and current drive (CD), particle balance maintenance, plasma wall interaction and the adequacy of equilibrium and stability control. A series of solutions to mitigate the challenges faced by long pulse H-mode plasmas are recently addressed in EAST.

These solutions encompass advanced plasma control strategies, innovative wall conditioning techniques, and optimized heating and current drive systems. The integration of these approaches has led to significant progress in sustaining high-performance plasmas over extended durations. Notably, EAST has achieved record-breaking pulse lengths and demonstrated enhanced confinement properties under reactor-relevant conditions. Furthermore, comprehensive studies on plasma-wall interactions have provided valuable insights into material erosion, fuel retention, and impurity control, which are crucial for the development of future fusion devices. The experimental findings from EAST not only validate theoretical predictions but also offer practical guidance for ITER's new research plan, bridging the gap between present-day experiments and the ultimate goal of commercial fusion power.

2. ACHIEVEMENTS OF LONG PULSE H-MODE OPERATION

On January 2025, EAST had made an important advance by achieving a record H-mode plasma over 1066-second with the total injected energy up to 3.05GJ. With this result, EAST has become the first tokamak that is capable to operate with a pulse length in thousand-second scale, with plasma temperatures in the tens of million degrees Celsius and sufficient self-driven current. Significant advancements have been made in the development of long-pulse H-mode on EAST in physics and technologies, as illustrated in Fig. 1. These include progress in radio frequency (RF) heating and current drive with low momentum input, tungsten handling strategy in a reactor-like metal wall, active control of divertor heat flux and particle exhaust, plasma wall interaction and particle balance, magnetic configuration and equilibrium stability in long duration.

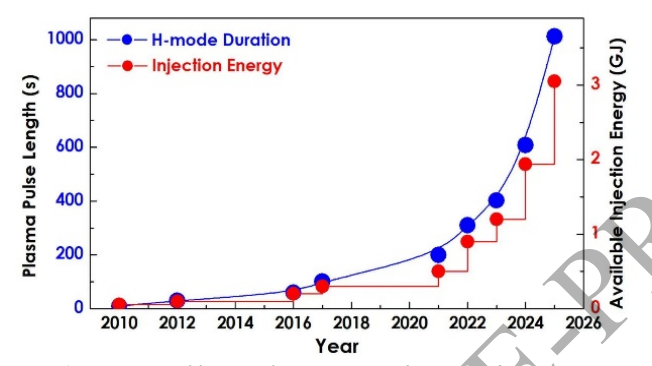


Figure 1 Progress of long pulse operation for H-mode in EAST.

A series of solutions to mitigate the challenges faced by long pulse H-mode plasma over 1066s pulse is shown in Fig. 2. The configuration is a lower single null, with the strike point on the tungsten divertor. Key parameters include: plasma current $I_p = 0.3$ MA, toroidal magnetic field $B_t = 2.5$ T, major radius R = 1.85 m, minor radius a = 0.45 m. A poloidal beta of $\beta_P = 2.0$ was achieved with a total RF power of 3 MW, including $P_{\text{LHCD}} = 1.1$ MW and $P_{\text{ECRH}} = 1.9$ MW. A fully non-inductive current drive with electron density at 60% of the Greenwald density, confinement enhancement factor H_{98y2} is greater than 1.3 due to the electron temperature internal transport barrier (e-ITB). A nature grassy ELM regime [2] was accessed with the outer strike point on the horizontal target, facilitating efficient RF power coupling and W source reducing due to sputtering/erosion. In addition, low-Z materials wall coating and real-time powder injections were applied to improve particle control capability. Thus, W impurity accumulation was not observed throughout the discharge, which is discussed in detail in the following section. These long-pulse operation capability, combined with steady-state plasma conditions, is projected to provide crucial scientific data and engineering validation for future commercial fusion power plants. Both scenarios incorporate sophisticated plasma control techniques, advanced heating and current drive systems, and optimized magnetic confinement configurations to achieve performance targets, as foreseen for the ITER Q \geqslant 5 long-pulse and steady state scenarios [3].

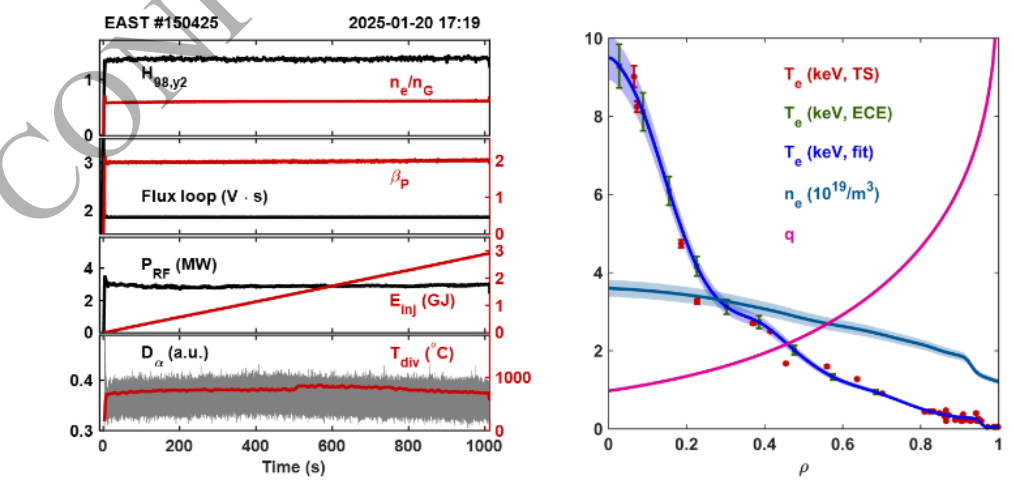


Figure 2 Time histories of EAST long-pulse H-mode discharge (Left), (a) $H_{98,y2}$ and normalized electron density n_e/n_G , (b) Poloidal flux and β_P , (c) RF power and total injected energy, (d) Divertor temperature (IR) and D_α emission. Electron density and temperature, current profiles (Right).

Transport analysis shows that a high bootstrap current fraction (calculated by ONETWO) f_{bs} of ~50% has been achieved, and it can be stably maintained in this extreme long pulse H-mode plasma. The peak of EC current density (and the EC power deposition as well) calculated by GENRAY/CQL3D code is very close to the plasma center. Most of the LH power is absorbed during the first pass and located at the region of $\rho \leq 0.6$ (see Fig. 3). The damping location of LH waves is sensitive to the electron temperature significantly. High electron temperature in the plasma core resulting from the very local ECRH was increased further due to the synergy effects between LH and EC waves.

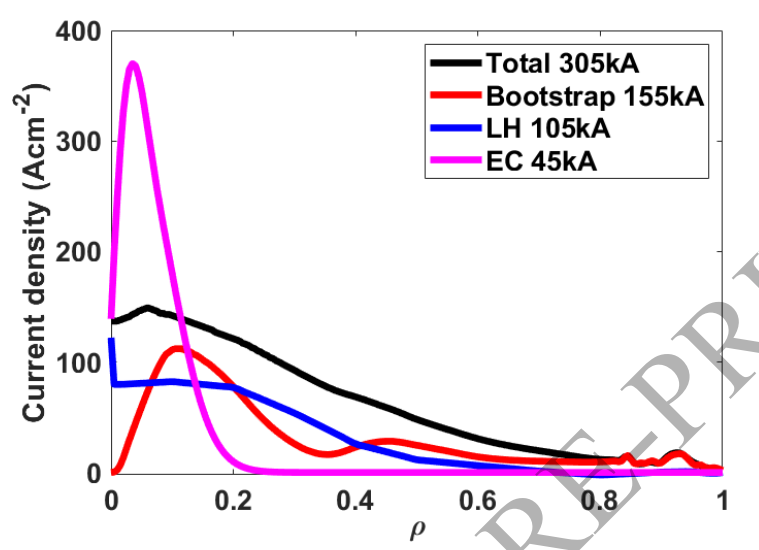


Figure 3 Current density profiles calculated from ONWTEO code.

Instead of zero loop voltage feedback control, a flux loop from the high field side mid-plane measured by a flux loop coil is newly applied for further improvement of feedback control with the actuator of lower hybrid current drive, seen from Fig. 4, ensuring fully non-inductive plasma. The target value of flux is specified with the measured flux at the onset of the feedback control. As expected, all currents in poloidal field coils remained stable, which reduced the alternating current loss in superconducting coils. Moreover, considering the coupling between the Ohmic current drive and the plasma shaping in superconducting tokamaks, the achievement of zero loop voltage and unchanged poloidal field coils currents ensured a truly steady-state plasma with precisely controlled shape. This experiment provided an innovative and promising control scheme which can integrate into the steady-state operation scenario in future fusion reactors.

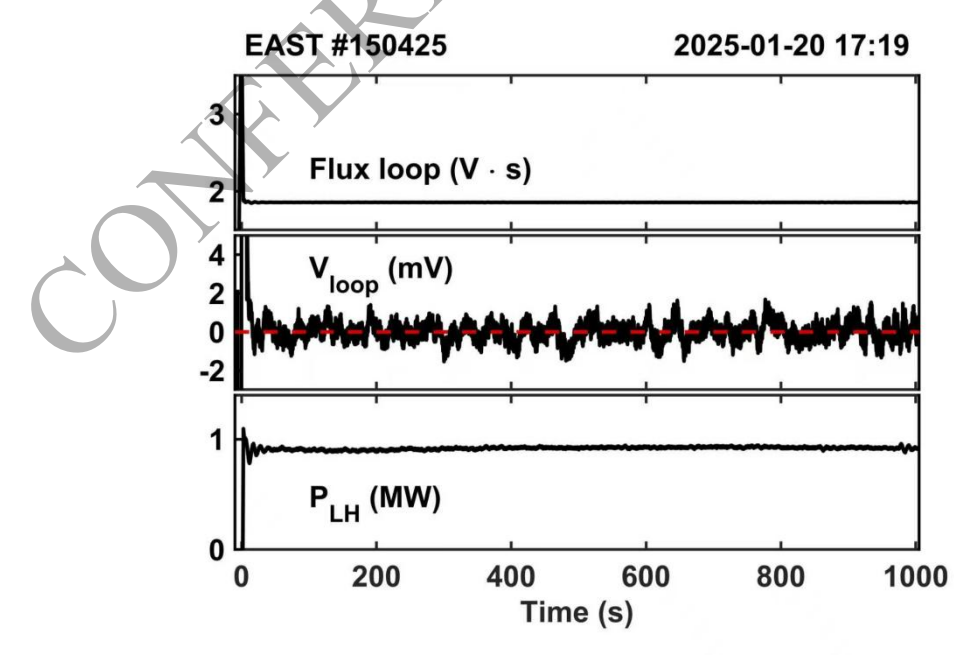


Figure 4 Newly developed innovative flux loop feedback control scheme using LHW current drive as the actuator on EAST.

3. SOLUTIONS TO CRITICAL ISSUES

3.1. Manipulating the synergy of ECRH and LHW to ensure high electron temperature gradient

The synergy effects between on-axis ECRH and LHCD play a crucial role in maintaining high confinement in electron channel. It enables the EAST program to address plasmas with high electron temperature gradient research. The synergy between ECRH and LHCD addressing the maintenance of the high confinement in electron channel allows the understanding of the abnormal energy fluxes driven by plasma turbulence and self-organized evolution of the ITB for fusion devices. The ITB in EAST discharge is nonlinearly self-organized, emerging near the magnetic axis in a positive magnetic shear heated plasma without momentum injection, which is long-term stability and promising ITB for ITER. The suppression of turbulence in the inner region of the ITB promises high confinement. Meanwhile, turbulence on the outer side of the ITB facilitates particle pump-out, thereby preventing the accumulation of tungsten impurity in the core. The long-term plasma performance indicates the reliability of this ITB structure.

On-axis power deposition leads to obtain a high confinement performance. For the oblique injection of EC waves in an up-shifted regime (co-current ECCD), an optimum value of toroidal field $B_T = 2.43$ T was confirmed experimentally by scanning the magnetic field slightly to realize high plasma confinement. For the 4.6 GHz-LHW, the optimum N_{\parallel} should be slightly higher than the $N_{\parallel}^{\rm acc}$, lower than which the wave accessibility becomes worse. However, too large N_{\parallel} will lead to a decrease in current drive efficiency ($\propto 1/N_{\parallel}^2$). The local accessibility condition $(N_{\parallel}^{\rm acc})$ in the plasma center with $n_{\rm e} \sim 3.6 \times 10^{19} \, {\rm m}^{-3}$ is ~ 2.0 . Consequently, the nominal $N_{\parallel} = 2.04$ of the 4.6 GHz LHW antenna [4] was chosen. This nominal value $(N_{\parallel} = 2.04)$ indicates that a strong Landau damping will take place at $T_{\rm e} \sim 10$ keV, according to linear damping condition $N_{\parallel} \approx 6.5/\sqrt{T_{\rm e}({\rm keV})}$ [5]. Since the electron temperature in the plasma core is close to 10 keV (namely, the spectral gap between the N_{\parallel} required for Landau damping and the launched N_{\parallel} is small), most of the LHW power is absorbed during the first pass. Thus, the LHW power loss in the scrape-off layer due to collisional absorption is negligible. Thanks to the high Te regime, the LHW CD efficiency defined as $\eta_{CD} \equiv I_{LH} R \bar{n}_e / P_{LH}$, is as high as $\sim 0.7 \times 10^{19} A/W/m^2$, where I_{LH} is the current driven by LHW waves, R the major radius, and P_{LH} the total power of the power spectrum. Besides, the coupling of LHW is mainly dependent on the electron density in the front of the antenna. If the electron density is lower than the cut-off value, the reflection coefficient will increase dramatically, while for too high electron density, the coupling will become worse as well. Thus, the LHW coupling may be tripped during the edge density perturbations induced by large ELMs. Thus, the grassy ELM regime with less edge density variation would be more favorable for LHW coupling.

3.2. Advanced magnetic measurements for precise control of the strike point location

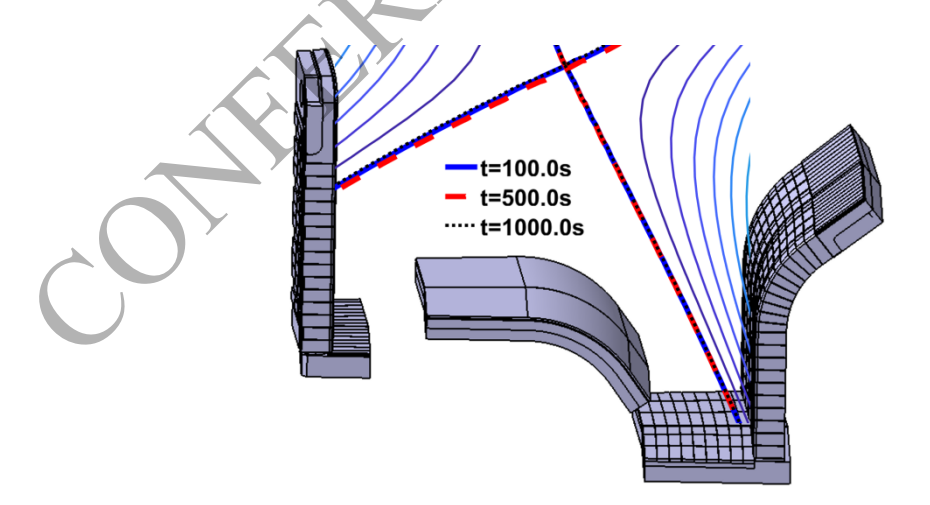


Figure 5 Precise control of strike point locations on lower divertor for thousand-second scale long duration operation.

The physics of equilibrium control for reactor-scale plasmas will rely on the same fundamental principles but will face additional challenges due to the long pulse duration, high neutron flux, thermal drifts of elevated temperatures. Recently, magnetic measurements for precise control of the strike point location long pulses have provided proof-of-principle demonstrations of control techniques in EAST. New low zero drift integrators are

developed and applied for the raw signal of magnetic measurements for this long pulse operation. The diagnostic exhibits a noise level of about 2 mT on the magnetic field, and 1mWb on flux loops allowing identifying the plasma boundary with an accuracy of one millimeter. The fiber optic current sensors without signal drift were used to measure the total plasma current and poloidal coils current compared with Rogowski coils and analog integrators. At the same time, the small linear drift of the integrators was real-time compensated in EAST plasma control system with daily test shots for the long pulse operation. The absolute positioning of the inner and outer gap has been precisely controlled and the divertor strike points shift within 2mm, seen Fig. 5, allowing the surface temperature well controlled under 800°C.

3.3. Impurity handling using low-Z material wall coating and real-time powder injection

During the long pulse discharges, impurity sources at both the mid-plane limiter and the divertor were effectively suppressed through real-time lithium wall conditioning, as shown in Fig. 6. The most intense impurity sputtering occurred around the equatorial plane on the limiter and at the strike point on the divertor's vertical target, where the incident particle flux was highest. Following the plasma start-up phase, light impurity sputtering (C, O, Li) near the divertor strike point decreased rapidly to a relatively low level, while the tungsten (W) sputtering rate began to rise. This evolution could be attributed to the degradation of the deposition layer on the divertor target formed during previous cleaning discharges. The subsequent increase in the intensity of all impurity lines at the target could be ascribed to a slight enhancement in plasma-wall interaction, which resulted in increased impurity release from the wall surface at the divertor target.

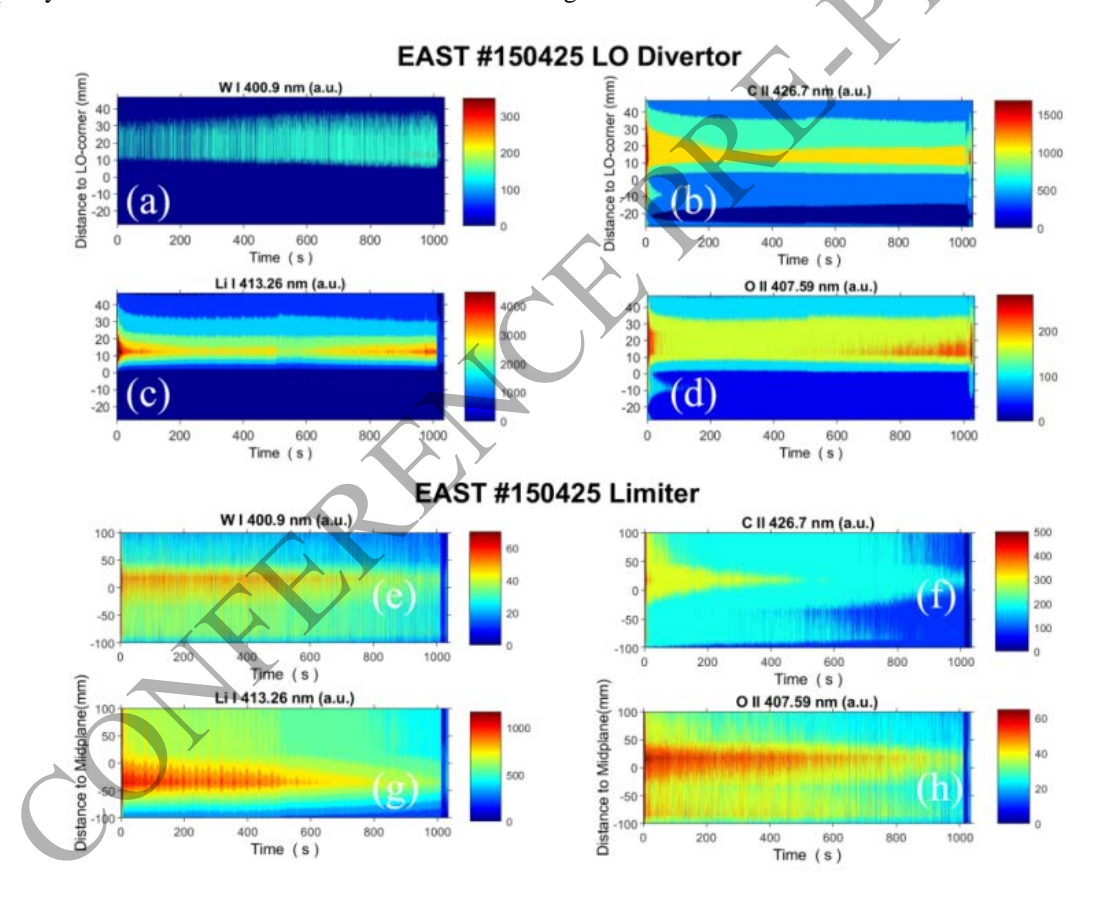


Figure 6 Temporal evolution and spatial distribution of impurity spectral line intensity along the limiter at low field side (a-d) and the lower outer divertor (e-h). The zero points on the vertical coordinate denote equatorial plane in (a-d) and the corner between horizontal and vertical targets in (e-h), respectively.

As indicated in Fig. 6(a-d), the decrease in impurity sputtering on the mid-plane limiter might be attributed to the cleaning effect of the main plasma on the limiter, which gradually reduced the impurity inventory on the wall surface. This reduction is beneficial for mitigating core impurity contamination. Furthermore, it can be observed in Fig. 6(c) that the intensity peak of the Li I line is situated below the equatorial plane, whereas the peaks for W I, C II, and O II lines are located above the equatorial plane. This discrepancy may be due to the non-uniform distribution of the lithium coating on the limiter's surface. A thicker lithium layer could more effectively suppress impurity sputtering.

The tungsten impurity concentration is shown in Fig. 7, as evaluated using the Tangential X-ray Crystal Spectrometer (TXCS) in the EAST tokamak. It can be seen that the tungsten impurity concentration follows a similar trend to the tungsten emission observed in the lower divertor region as shown in Fig. 6(g), with both increasing slightly over the course of the discharge. However, throughout the entire discharge duration, the tungsten concentration remained at a very low level of $\sim 10^{-5}$, likely due to the effects of lithium wall conditioning and nature grassy ELM regime to reduce tungsten source along with high core electron temperature gradient to enhance particle outward transport. This low tungsten concentration, in turn, ensures both high plasma confinement and much prolonged discharge duration in EAST plasma operation.

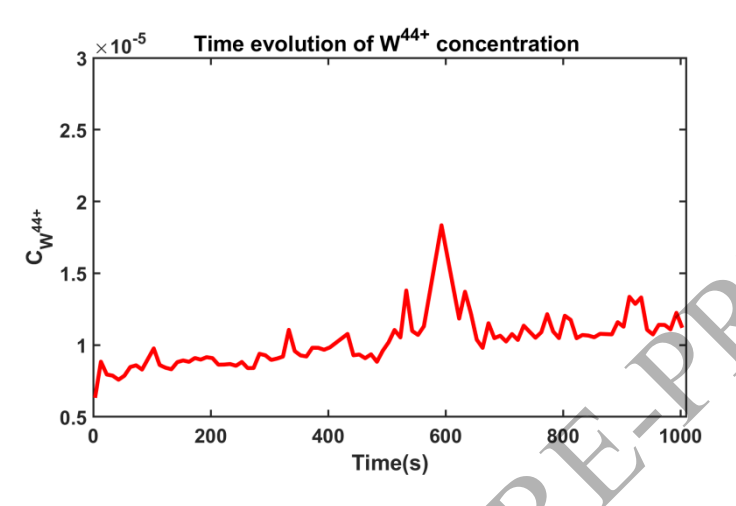


Figure 7 Tungsten impurity concentration in the long pulse discharge.

3.4. Edge recycling and particle exhausting control

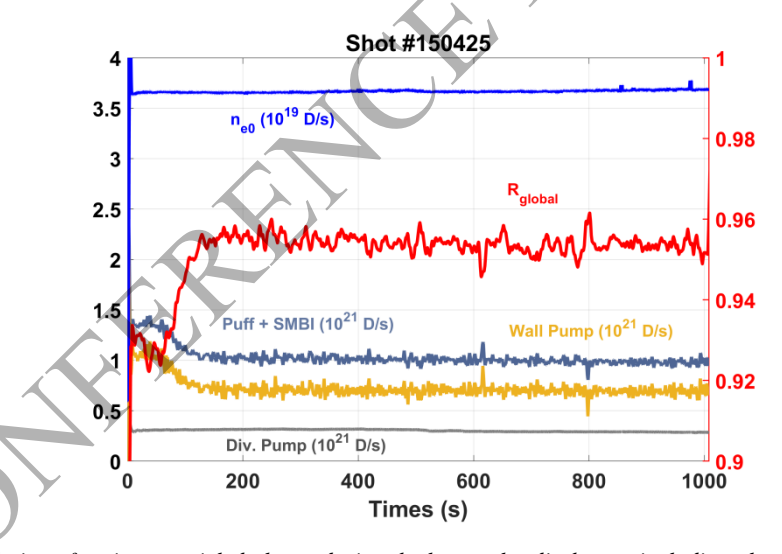


Figure 8 Time evolution of various particle balance during the long pulse discharge, including plasma density (ne), external gas injection rate including gas puffing and Supersonic Molecular Beam Injection (Puff + SMBI), divertor pumping rate via cryopumps (Div. Pump), and wall pumping rate (wall pump), and global recycling coefficient ($R_{\rm global}$).

Fuel recycling was effectively controlled throughout the long-pulse discharge. The plasma density remained constant at a moderate value of 3.0×10^{19} m⁻³, as shown in Fig. 8, and demonstrated exceptional stability over the entire discharge. Particle balance analysis revealed that during the initial 150 seconds, both the external gas injection rate and wall pumping rate were higher than in later phases. This is attributed to the relatively fresh wall surface and enhanced wall pumping capability at the beginning of the discharge. After approximately 150 seconds, the external gas injection, divertor pumping, and wall pumping rates stabilized. The total gas puffing and SMBI injection rate was measured at ~ 1.0×10^{21} D/s, while the pumping rate via the divertor cryopump was ~ 0.3×10^{21} D/s, and the wall pumping rate was ~ 0.7×10^{21} D/s. These values indicate that the wall pumping played a more significant role in recycling control compared to the divertor cryopumps, likely due to the extensive lithium

coating and real-time lithium injection. Additionally, the effective control of fuel recycling can be attributed to precise plasma magnetic shape control and careful management of the divertor heat load.

The global recycling coefficient (R_{global}), defined as the ratio of effective fueling due to recycled particles to the total particle flux from the plasma to the wall, was maintained nearly constant at 0.95 throughout the discharge. This indicates that the global plasma particles were under excellent control. This achievement marks a significant milestone: for the first time in long-pulse operations of magnetically confined plasmas, such precise particle control has been sustained during an H-mode plasma operation exceeding 1000 seconds. Furthermore, these findings provide valuable insights into recycling control, suggesting that a global recycling coefficient of approximately 0.95 may represent an optimal condition for maintaining both excellent plasma confinement performance and extended operational duration.

The wall materials evolution has been investigated by plasma-wall integrated modeling. The results reveal that a lithium (Li)-enriched layer can develop underneath the surface of the divertor's tungsten material. This multilayered structure significantly influences local particle recycling processes, thereby affecting the distribution of edge plasma. Experimental results show that the intensity peak of Li I line is situated below the equatorial plane, the decrease in impurity sputtering on limiter, which gradually reduced the impurity inventory on the wall surface. To study the Li coating influence on the edge particle recycling from tungsten wall material, SOLPS-SDTRIM.SP-DIVIMP integrated modeling framework has been developed. Based on EAST typical discharges, the Li erosion and transport have been simulated. Results reveal that a 50 nm Li overlayer on divertor W surface diminished in several seconds, and the evolution of the surface material shows significant impact on the D recycling through changing the D reflection rate and reemission rate. Therefore, material evolution must be considered for D recycling study.

4. KEY PHYSICS UNDERSTANDING

4.1. Self-regulating mechanism to sustain T_e-ITB

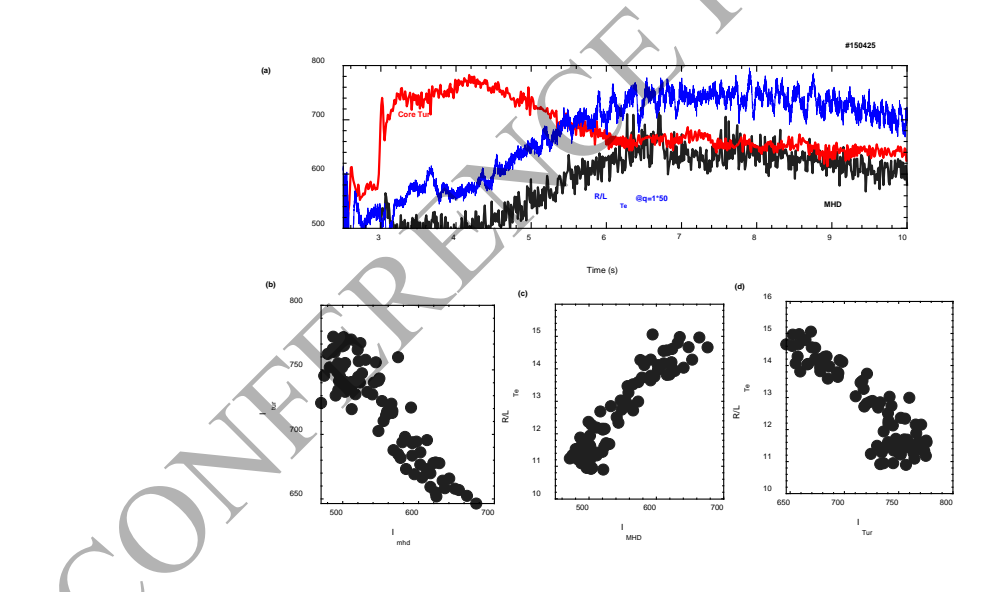


Figure 9 The interaction of MHD and turbulence in the core region of #150425. (a) evolution of turbulence, MHD and R/L_{Te} . (b) I_{MHD} VS I_{tur} ; (c) I_{MHD} VS R/L_{Te} ; (d) I_{tur} VS R/L_{Te}

Fig. 9 investigates the dynamic interplay between electron temperature gradient (ETG) turbulence and a magnetohydrodynamic (MHD) mode with $\frac{R}{L_{Te}}$ >10. Following an increase in ECRH power at t=3s, the core plasma is continuously heated, driving the $\frac{R}{L_{Te}}$ above a critical threshold of 9. This triggers the rapid growth of core ETG turbulence [6], as measured by CO₂ laser scattering diagnostics with a characteristic wavenumber of $k\rho_s \sim 10cm^{-1}$ [7]. However, as R/L_{Te} further increases, a significant shift in plasma behavior is observed: an m/n=1/1 MHD mode, localized at the q=1 rational surface, begins to grow [8]. Concurrently, the amplitude of the pre-existing ETG turbulence is markedly suppressed. Statistical analysis of the turbulence amplitude, the 1/1 mode intensity, and R/L_{Te} (Fig. 9b-d) reveals a clear anti-correlation between the 1/1 mode and ETG turbulence. This confirms

a direct competitive relationship. Furthermore, the data shows a positive correlation between the 1/1 mode intensity and R/L_{Te} , and a negative correlation between ETG turbulence and R/L_{Te} . After t=6s, both the ETG turbulence and the m/n = 1/1 mode saturate, and the system settles into a new quasi-steady state where R/L_{Te} is maintained at an elevated value of approximately 13. We propose that the interaction between the saturated m/n=1/1 mode and the residual ETG turbulence, potentially mediated by a self-generated current, creates a self-regulating mechanism. This mechanism is responsible for sustaining the high-performance, high-gradient plasma core, demonstrating a novel pathway to achieving improved confinement.

4.2. Magnetic shear tailoring by ECCD

By adjusting the ECRH mirror, the power deposition was shifted from the core to the edge region during H-mode operation, resulting in a reduction of plasma density and tungsten impurity levels while simultaneously steepening the electron and ion temperature profiles. The PCR diagnostic detected an electrostatic turbulence propagating in the ion diamagnetic direction at the measurement location of $\rho_t \approx 0.3$ -0.5, as shown in Fig. 10. Following the ECRH injection, the intensity of the low-frequency broadband turbulence gradually decreased from ~3.8s to ~5.5s. During this period, both the core electron (red line) and ion temperature (red dot) exhibited a gradual increase, while the core plasma density and tungsten impurity gradually decreased. Cross-power spectral analysis during the interval t = 3.5 - 4.5s revealed that the turbulence frequency spectrum peaked near zero frequency and propagated in the ion diamagnetic direction. These characteristics suggest that the observed turbulence is attributed to ITG instability. And, the reduction in its intensity starting at ~3.8s is probably caused by the onset of negative magnetic shear at the core. Note that the measurement position of the PCR diagnostic is dependent on the plasma density, which shifted from $\rho_t \sim 0.5$ to $\rho_t \sim 0.3$ as the plasma density gradually decreased from ~4.2s to ~5.5s during the experiment.

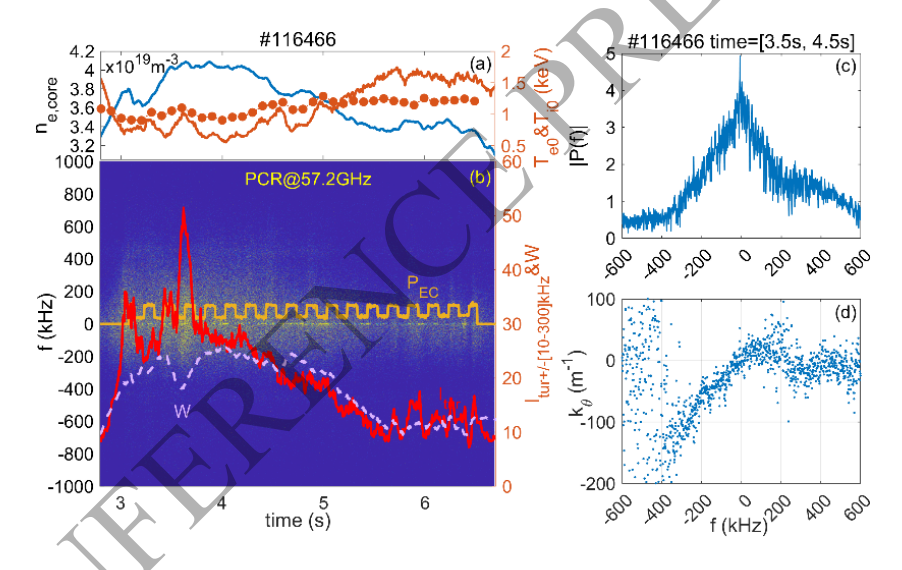


Figure 10 Temporal evolution of (a) line-averaged plasma density (blue line), core ion (red dot) and electron temperature (red line); (b) turbulence power spectrum and its intensity (red line) at core plasma for channel 57.2GHz, ECRH power (yellow line) and tungsten impurity (purple dashed line); Ensemble-averaged spectra over the interval t = [3.5, 4.5] s of (c) turbulence power and (d) wave-number.

5. JOINT EXPERIMENTS IN SUPPORT OF ITER NEW RESEARCH PLAN

5.1. Optimization boronization and characterization impact on operation

In support of the R&D requirement for the ITER new research plan, a dedicated set of joint ITER-EAST experiments have been performed on optimization and characterization of boronization, plasma start-up on the tungsten limiter, and the impact of W on the H-mode operational space with and without boron-coatings, make significant contributions to the ITER database. Both of $C_2B_{10}H_{12}$ and $C_2B_{10}D_{12}$ were used as working material for boronization, and the $C_2B_{10}H_{12}$ was heated up to 80-100 °C assisting with D/He ICWC and GDC. After each boronization, D/He cleaning was continued for 30-120 minutes to remove co-deposited hydrogen in boron films. Comparing to GDC and 45kW ICWC boronization technology,

the 200kW ICRF-assisted method was found to improve plasma uniformity and boron deposition rate. In particular, the uniformity performance could be enhanced with increasing toroidal field.

The dedicated tungsten limiter start-up experiments aim to provide direct experimental database for code validation. Like many tokamaks, the ITER plasma will start up on the central column for a rather long period of \sim 10s, where tungsten material is fully exposed. The impact of tungsten on the start up phase leads to more concerning. On EAST, a range of plasma current and density platform was chosen to carry out the experiments with assisting of ECRH on breakdown, by staying the plasma as long as possible on the ITER-like tungsten monoblock outboard limiter [9]. A significant observation is that the total radiated power ultimately reaches a saturation level at both densities, equating to approximately 0.4 MW, which corresponds to $f_{\rm rad}$ of around 0.6. This outcome strongly suggests the presence of a self-regulating sputtering mechanism. A second key finding is that sufficient on axis electron heating is crucial for sustaining stable plasma operation in this limiter phase.

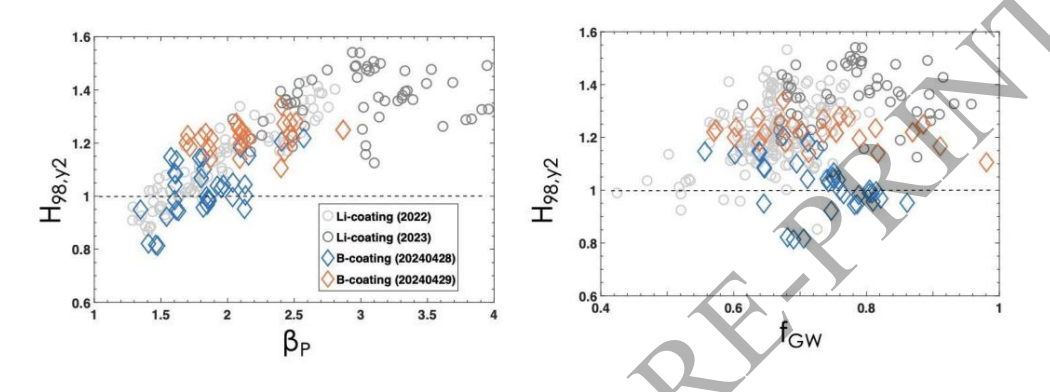


Figure 11 Comparison of energy confinement versus poloidal beta (left) and normalized density (right) for lithium coating and boronization wall.

The impact of tungsten limiter on H-mode performance were evaluated for low/no boron-film and fresh boronization conditions respectively in the high q_{95} plasmas under strong on-axis ECRH heating. Based on the experimental observation, the type-II ELMs H-mode plasmas were found to provide higher confinement and lower plasma radiation than those with type-I ELMs. With boron coverage on the tungsten limiter, the plasma performance with 1.5MW ECRH is comparable to that of 3MW ECRH without boronization [10]. In general, the energy confinement with boron-wall is normally reduced by $10\sim15\%$ comparing to those with lithium coating, seen Fig. 11.

5.2. Compatible divertor detachment and ELM control via RMP

Effective Type-I ELM suppression has been achieved using n = 2 RMP, these results verify a good compatibility of radiative divertor operation by injecting nitrogen (N_2) . With a rotated RMP field, the spiral pattern was observed in the particle and heat fluxes on the divertor target. These patterns are aligned with simulated divertor footprints contours. With the onset of N_2 puffing, N-II radiation rapidly increased and then saturated. And a significant drop in heat flux marked the onset of power detachment. The electron temperature measured from the LO-divertor vertical target revealed that both the near and off-separatrix lobes decreased from ~20 eV to below 5 eV, indicating strong temperature detachment. With the background plasma in a full metal wall and tungsten divertors, both energy and particle confinement were well maintained during both RMP application and the radiative divertor operation phases. The tungsten concentration in the core plasma decreases after the application of RMPs and drops further upon achieving detachment. With the application of RMPs and nitrogen seeding, the dominant radiation shifts from core to the plasma edge region. The observed decrease in tungsten radiation is directly associated with the reduction in tungsten peaking in the core plasma. These results show the potential compatibility of RMP ELM control and divertor detachment on both original and splitting strike lines, although only ELM mitigation was achieved here. A lower density limit for accessing ELM suppression using n=4 RMP was also observed. The application of RMPs significantly reduced the density pedestal height, while during ELM suppression, the pedestal foot was elevated, indicating a change in the primary transport region. Stability analysis of peeling-ballooning modes (PBMs) using the ELITE code shows that as ELM is suppressed, PBMs gradually enter the most stable region, which is consistent with the experimental results.

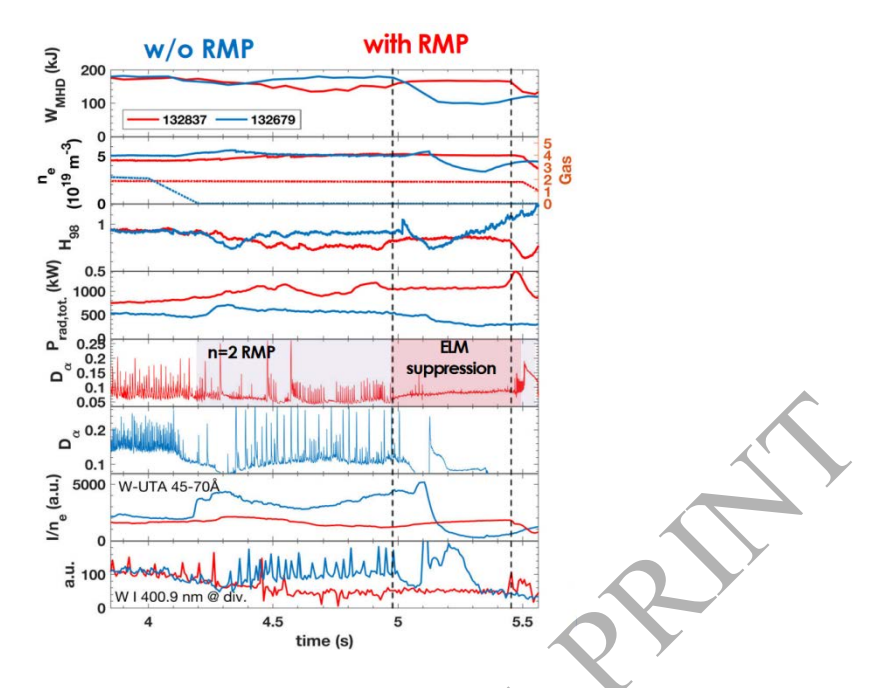


Figure 12 Realization of ELM suppression using n=2 RMPs with decreased W level and small effects on plasma energy and density.

The core-edge integration in high performance steady-state operation scenarios with metallic wall compatibility has also been explored experimentally. A stationary ELM-free H-mode regime sustaining for 50 seconds with simultaneous feedback-controlled divertor detachment has been demonstrated on EAST recently. After nitrogen impurity injection, the electron temperature and surface temperature of the divertor target plate decreased significantly, entering a partially detached state. A high-frequency turbulence mode of ~600 kHz existed in the steep gradient region of the pedestal, assisting in particle removal and preventing impurity core accumulation and ELM bursts.

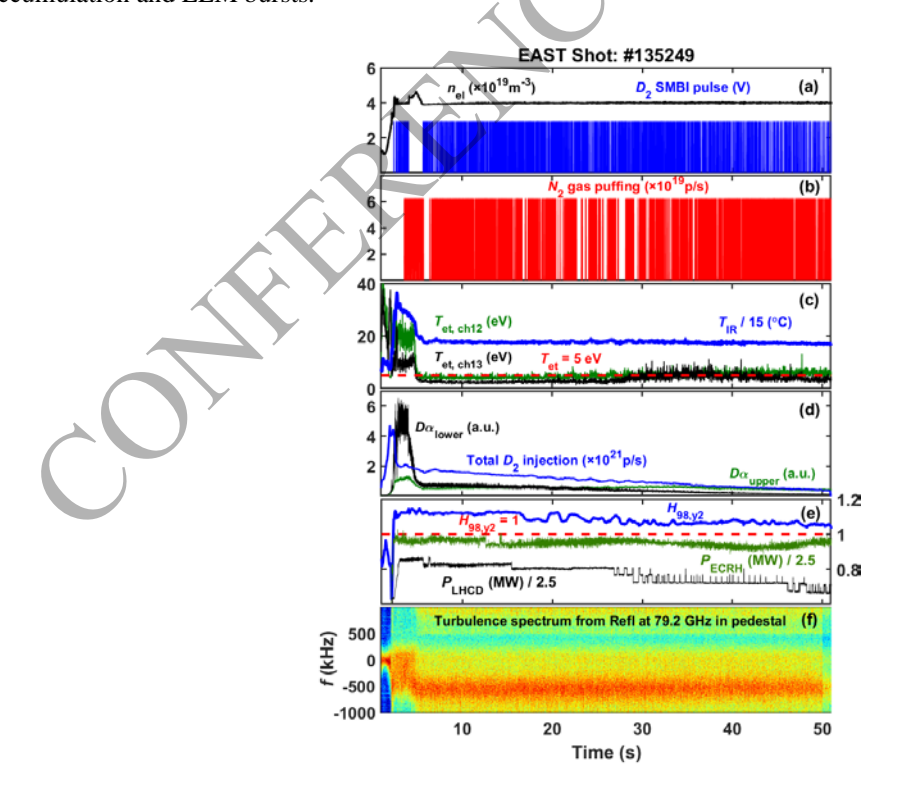


Figure 13 Demonstration of divertor detachment and ELM-free long-pulse discharge enabled by HFBT-assisted particle exhaust

5.3. High ion temperature experiments

Furthermore, to improve plasma fusion performance with W-Divertor/W-limiter utilizing B-coating, experiments have been done on EAST with dominant ion heating by combining high power NBI and impurity seeding. It is found that the central ion temperature (Ti) can be increased to ~10keV at moderate density. In this high-T_i peak regime, multi-scale instabilities have been observed to provide a clear picture of the interaction between turbulence behaviors and impurity transport in the plasma core. Long-Lived Modes (LLMs), driven by the hot-ion population, exhibited a broad frequency spectrum ranging from 20 kHz to 500 kHz. Their spatial characteristics were also diverse, spanning scales from macroscopic kink-like modes to ion-scale turbulence. Analysis revealed a dominant fishbone mode with a prominent n = 2 harmonic [11]. Soft X-ray (SXR) tomography provided critical insights into their spatial structure: the fundamental n = 1 component displayed a broad radial profile, extending outward to approximately $\rho \sim 0.7$ (the location of the q = 2 rational surface). Weaker amplitude Beta-induced Alfvén Eigenmodes (BAEs) were detected in the frequency range of 100-200 kHz. Notably, these BAEs were observed to disappear during periods dominated by LLM activity, suggesting a complex interaction or suppression mechanism between these modes [12]. Furthermore, a significant competitive relationship was identified between ion-scale turbulence (f = 200-1000 kHz) and the fishbone instabilities. This competition is likely linked to the fishbone-induced poloidal plasma rotation [13]. It is hypothesized that the fishbone modes trigger a sheared poloidal flow, which in turn suppresses the ion-scale turbulence. This suppression mechanism is believed to play a crucial role in sustaining and reinforcing the T_i -ITB, thereby contributing to the overall performance of the hot-ion regime.

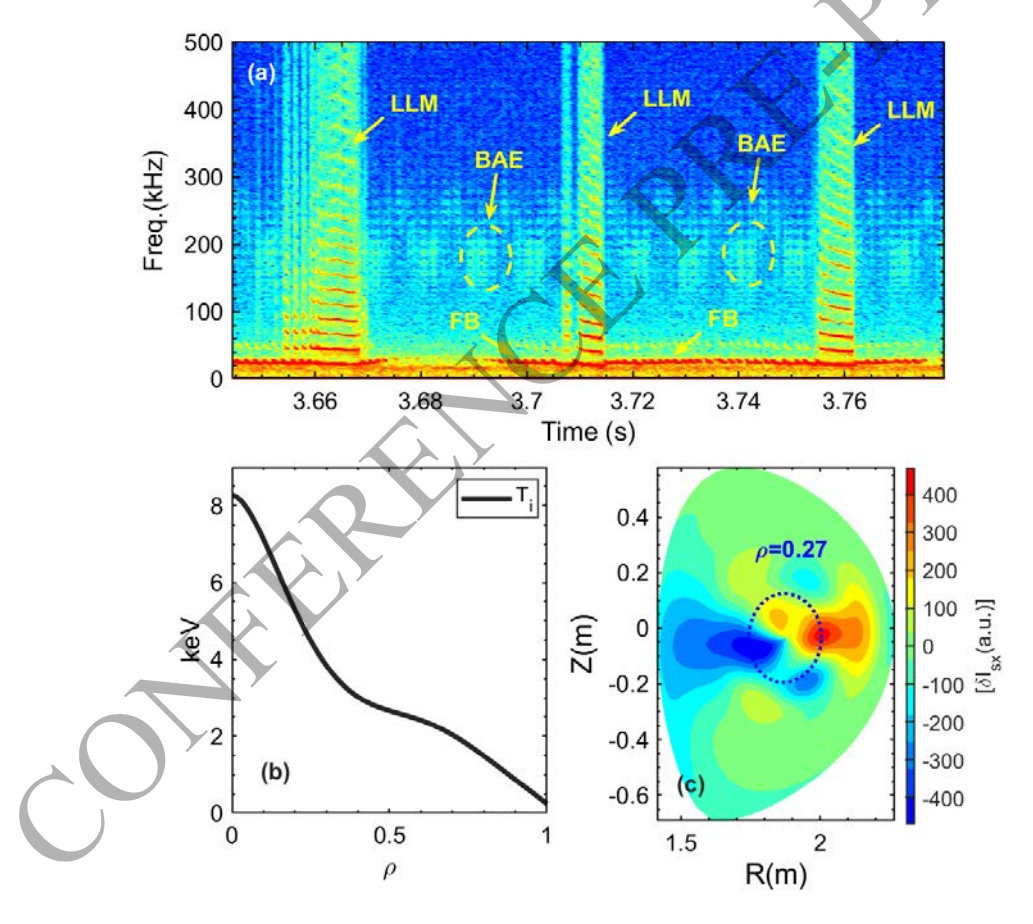


Figure 14 Multi-scale instabilities observed in EAST T_i -ITB region for shot #136377. (a) Spectrogram of edge Mirnov coils. (b) T_i (c) SXR tomographic reconstruction of FB.

6. FUTURE PLAN AND SUMMARY

A significant upgrade has been implemented on EAST to expand the plasma volume on the low-field side. This upgrade involves transforming the upper divertor into a redesigned BEST-like cooling structure with a power

handling capacity of 12 MW/m². Concerning heating and current drive (H&CD), a series of parallel upgrades have been conducted. A 4.6 GHz PAM launcher with active cooling for a new 4 MW LHW system is under development to enhance the long-distance current drive (CD) capability [14]. A triple current strap antenna has been adopted for the ion cyclotron resonance frequency (ICRF) system to reduce the electric field in the antenna limiter, thereby suppressing tungsten impurity radiation induced by sputtering. Two additional gyrotrons for the ECRH system will increase the total power output capability at 140GHz frequency to 4.5 MW for up to 1000s of operation. These improvements will significantly enhance EAST's capacity to focus more on core-integration research for ITER and BEST steady-state scenarios with a full metal first wall. Meanwhile, the EAST program will continue to promote international joint research and experiments to accelerate the development of fusion energy.

Remarkable advancements have been achieved in the field of long-pulse steady-state H-mode operation on EAST. High-performance long-pulse H-mode plasmas have been successfully demonstrated under conditions that closely resemble those of future fusion reactors, including the implementation of a reactor-like metal wall, operation with low momentum input, and utilization of an electron-dominated heating scheme. These breakthroughs represent significant milestones in the pursuit of practical fusion energy. Furthermore, a comprehensive set of innovative solutions to overcome the various technical challenges associated with maintaining stable long-pulse H-mode plasmas have systematically developed and implemented, paving the way for more reliable and sustained fusion reactions in future reactor-scale devices.

ACKNOWLEDGEMENTS

Work was supported in part by the National MCF Energy R&D Program 2022YFE03050000.

REFERENCES

- [1] GONG, X., Overview of recent experimental results on the EAST Tokamak, Nucl. Fusion 64 (2024) 112013.
- [2] XU, G.S., YANG, Q.Q., YAN, N., et al., Promising High-Confinement Regime for Steady-State Fusion, Phys. Rev. Lett. **122** (2019) 255001.
- [3] GORMEZANO, C., SIPS, A.C.C., LUCE, T.C., et al., Chapter 6: Steady state operation, Nucl. Fusion 47 (2007) S285-S336.
- [4] LIU, L., LIU, F.K., JIA, H., et al., 4.6-GHz LHCD Launcher System of Experimental Advanced Superconducting Tokamak, Fusion Sci. Technol. **75** (2018) 49-58.
- [5] BRAMBILLA, M., Electron Landau damping of lower hybrid waves, Nucl. Fusion 18 (1978) 493.
- [6] LI, E., ZOU, X.L., XU, L.Q., et al., Experimental Evidence of Intrinsic Current Generation by Turbulence in Stationary Tokamak Plasmas, Phys. Rev. Lett. **128** (2022) 085003.
- [7] LI, P., LI, Y.D., LI, J.G., et al., Study of turbulence modulation and core density peaking with CO2 laser collective scattering diagnostics in the EAST tokamak, Nucl. Fusion **60** (2020) 066001.
- [8] XU, L., LIN, S., MAI, C., et al., Observation of fast electron redistribution during saturated kink mode in high βp H-mode discharge with central heating in EAST tokamak, Nucl. Fusion **64** (2024) 046024.
- [9] PITTS, R.A., LOARTE, A., WAUTERS, T., et al., Plasma-wall interaction impact of the ITER re-baseline, Nucl. Mater. Energy 42 (2025) 101854.
- [10] LOARTE, A., PITTS, R.A., WAUTERS, T., et al., The new ITER baseline, research plan and open R&D issues, Plasma Phys. Control. Fusion **67** (2025) 065023.
- [11] XU, L., ZHANG, B., LIN, S., et al., Multi-scale core-edge instabilities and particle acceleration unveiled in EAST ion temperature peak discharge, Nucl. Fusion (2025)
- [12] SHEN, W., XU, L.Q., QIU, Z.Y., et al., Investigation of double frequency fishbone in EAST with neutral beam injection, Nucl. Fusion **65** (2025) 066012.
- [13] BROCHARD, G., LIU, C., WEI, X., et al., Saturation of Fishbone Instability by Self-Generated Zonal Flows in Tokamak Plasmas, Phys. Rev. Lett. **132** (2024) 075101.
- [14] LI, M.H., LIU, L., YANG, Y., et al., Design and analysis of a PAM launcher at 4.6 GHz for a new LHCD system on EAST, Nucl. Fusion 64 (2024) 036017.